ANALYSIS OF DEFECTIVE HYDROSTATIC RADIAL BEARINGS FOR FIVE MEGAJOULE HOMOPOLAR GENERATOR

H. G. Rylander, and W. F. Weldon

Presented at the
ASME Winter Annual Meeting,
1980 Technical Session

Publication No. PR-11
Center for Electromechanics
The University of Texas at Austin
Balcones Research Center
EME 1.100, Building 133
Austin, TX 78758-4497
(512)471-4496

ANALYSIS OF DEFECTIVE HYDROSTATIC RADIAL BEARINGS FOR FIVE MEGAJOULE HOMOPOLAR GENERATOR

H. G. Rylander, W. F. Weldon

Center for Electromechanics
College of Engineering
The University of Texas at Austin
Taylor Hall 167
Austin, Texas 78712

ABSTRACT

Hydrostatic bearings were designed for a five megajoule homopolar generator since they offered the advantages of low shaft friction, high load capacity and high stiffness independent of shaft speed. The original bearings were satisfactory except for electrical pitting. A redesign using a high pressure laminated (G-9) fiberglass cloth reinforced melamine-formaldehyde resin composite resulted in a defective design. Design parameters are given with a complete analysis showing where the design was defective along with a satisfactory solution used in a subsequent redesign.

INTRODUCTION

Pulsed power devices needed to confine and heat plasma are basically energy storage systems capable of receiving and storing energy at low power levels over a relatively long period of time, then delivering upon demand the stored energy at much higher rates. Storage batteries, capacitors, and inductive devices are the usual choice for experiments or applications requiring large pulses of electrical power delivered in a short time period. Inertial energy storage in a flywheel driving a homopolar generator (Faraday Disk) is quite competitive in that it is less expensive, more compact, efficient, and reliable. Such a device was designed and built in 1972 but it suffered from several design deficiencies.

This first machine did not have sufficient motoring power to come up to speed because of the use of conventional (AISI-E52100) steel ball bearings. These bearings were operating in a high magnetic field which unfortunately resulted in a factor of ten increase in rolling friction.

A second generation homopolar generator, as shown by schematic in Figure 1, was designed and built in 1974 by The University of Texas Center for Electromechanics to demonstrate the feasibility of inertial energy storage using homopolar conversion. As originally designed it was to produce 165 kA from a speed of 5600 rpm. A steel (AISI 4340) rotor 61 cm in diameter, 28 cm thick, weighing 730 kg operates in a 1.6 T axial magnetic field. Hydrostatic bearings were selected for this machine. Design improvements reduced the machine's low internal impedance, mostly by an improved mechanical brush mechanism, such that it produced 560 kA from 2800 rpm (half speed) stopping the rotor in 0.7 sec. After repeated discharges in the short circuit mode proved its basic reliability, the machine was connected to various loads such as an inductive storage coil and welding experiments with 2-inch mild steel pipes.

Upon completion of these experiments, the hydrostatic bearings had deteriorated such that the machine could not be motored to full speed with full field strength. Misalignment, out-of-roundness and a general loss of pressure reduced the radial stiffness such that the machine could not operate safely at high speeds. Since the machine was to be used in an upcoming 4-inch stainless steel pipe resistance welding program requiring many high level discharges, it was decided to disassemble the machine for inspection and rebuild to obtain higher performance.

Disassembly of this machine revealed definite signs of distress in the radial bearings. Inspection showed electrical pitting on the lands as shown in Figure 2. Electrical pitting was also found on the shaft. The effects of pitting on performance are such that the effective radial clearance is increased resulting in a decrease in load capacity and stiffness.

Since the 5 MJ homopolar machine was designed as an experimental device, it had several mechanical and electrical elements that were designed to operate at or beyond present levels of technology. However, it is the purpose of this paper to investigate the design of the radial hydrostatic bearings for this machine with emphasis on defective design using a new bearing material, high pressure laminated (G-9) fiberglass cloth reinforced melamine-formaldehyde resin composite.

Bearing Selection

Three types of bearings, rolling element, hydrodynamic and hydrostatic were considered for this design which was required to meet the following constraints:

1. Electrical current must flow through the shaft at the bearing location. Shaft size must be at least 12.5 cm (5 in.) in diameter to carry this current.
2. Large shaft size results in much higher surface speeds (37 m/sec or 122 ft/sec) in the bearings than would normally be used on a rotor of the same size and weight.
3. Low shaft friction will reduce motoring time.
4. Full stiffness is required at zero speeds. Bearing loads at zero speed are as large as at full speed.
5. Electrical insulation is necessary to prevent pitting and reduce circulating currents in the bearings during discharge.

Hydrostatic bearings are capable of meeting all five constraints stated above whereas other types will fail to meet one or more of these requirements.

Hydrostatic Bearing Design

A computer program based on a mathematical model was developed to aid in the design of these bearings. Operating characteristics such as load capacity, flow rates, pocket pressures, and deflection were obtained for specific bearing designs conforming to the general geometric layout as shown in Figure 3.

Throughout the discussion of the bearing performance prediction techniques the following nomenclature is used: refer to Figure 3.

- L_p - pocket length in the axial direction
- ℓ - circumferential land width
- ℓ_c - axial land width
- D - journal diameter
- R - journal radius = D/2
- C - radial clearance
- d_o - orifice diameter
- P - pressure
- P_o - supply pressure
- P_a - ambient pressure
- e - eccentricity
- E - eccentricity ratio = e/c
- L - axial bearing length
- L_D - pocket length in the circumferential direction
- ρ - oil density
- μ - oil viscosity
- c_d - orifice discharge coefficient
- t,b,s - subscripts meaning top, bottom, side respectively
- Q - volumetric flow rate of oil
- θ - angular coordinate around the circumference, positive counterclockwise from the top vertical
- x - linear coordinate around circumference = $R\theta$
- W - bearing load capacity

The vertical resultant force exerted on the journal by the pressure field when the shaft is displaced toward the bottom pocket by a distance e is called the load capacity. Qualitatively, one can reason the existence of such a force since the increased restriction of the flow from the bottom pocket due to e reduces the flow to that pocket and allows the pocket pressure to increase toward the supply pressure. The reverse process occurs at the top pocket location, and therefore, P_t decreases. This creates a situation such that $P_b > P_t$ and a resultant vertical force on the journal is produced. The side pockets do not greatly affect the load capacity but must be present to allow the bearing to support loading from any direction.

Conceptually the calculation of the bearing capacity is very simple, however, the geometry of the pockets, lands and clearances adds a great deal of algebraic complexity to the problem. In summary the flow continuity of the system is satisfied, thus determining the pressure in the bottom, side and top pockets for a given eccentricity, e, or eccentricity ratio, E. The resultant force is then calculated by integrating the vertical components of the differential forces exerted on the journal by the pressure field.

Let Q_{ij} represent the volumetric flow rate of oil entering the ith pocket to the jth sink. Then continuity of flow for the pockets can be represented by

$$\text{Bottom Pocket} \quad Q_b = Q_{ba} + 2Q_{bs}$$

$$\text{Top Pocket} \quad Q_t = Q_{ta} + 2Q_{ts}$$

$$\text{Side Pocket} \quad Q_s = Q_{sa} + Q_{st} + Q_{sb}$$

where b, t, s, a denote bottom, top, side and atmosphere respectively. It should be noted that $Q_{ij} = -Q_{ji}$. Total flow rate Q_T is given by

$$Q_T = Q_b + Q_t + 2Q_s$$

Let us now define the following nondimensional parameters:

$$\bar{Q} = \frac{Q}{\left(\frac{C^3 R P_o}{3\mu\ell}\right)}$$

$$\lambda = \frac{3\pi c_d d_o^2}{4C^3}\left(\frac{\ell}{L_p}\right)\left(\frac{L_p}{R}\right)\mu(2/\rho P_o)^{1/2}$$

$$m = \left(\frac{\ell}{\ell_c}\right)\left(\frac{L_p}{R}\right), \quad \bar{\theta} = \frac{L_D}{2R}$$

$$\bar{P} = \frac{P}{P_o}, \quad \bar{W} = \frac{W}{RL_p P_o}$$

$$A = \left\{\frac{\pi}{4} - \frac{3}{\sqrt{2}}E + \frac{3\pi + 6}{8}E^2 - \frac{5}{6\sqrt{2}}E^3\right\}$$

$$B = m\left\{\frac{[1 - E\cos\bar{\theta}]^2 \quad [1 - E\sin\bar{\theta}]^2}{2 - E[\cos\bar{\theta} + \sin\bar{\theta}]}\right\}$$

$$D = \left\{ \frac{\pi}{4} + \frac{3}{\sqrt{2}} E + \frac{3\pi + 6}{8} E^2 + \frac{5}{6\sqrt{2}} E^3 \right\}$$

$$E' = m \left\{ \frac{[1 + E\cos\bar{\theta}]^2 \quad [1 + E\sin\bar{\theta}]^2}{2 + E[\cos\bar{\theta} + \sin\bar{\theta}]} \right\}$$

$$F = \frac{\pi}{2} + \frac{3E^2}{4} (\pi - 2)$$

The flow through the ith orifice allows one to write

$$\bar{Q}_i = \lambda\sqrt{1 - \bar{P}_i}$$

The flow equations in terms of the above dimensionless parameters become

$$\lambda\sqrt{1 - \bar{P}_b} = A(\bar{P}_b - \bar{P}_a) + B(\bar{P}_b - \bar{P}_s)$$

$$\lambda\sqrt{1 - \bar{P}_t} = D(\bar{P}_t - \bar{P}_a) + E'(\bar{P}_t - \bar{P}_s)$$

$$\lambda\sqrt{1 - \bar{P}_s} = -B(\bar{P}_b - \bar{P}_s) - E'(\bar{P}_t - \bar{P}_s) + F(\bar{P}_s - \bar{P}_a)$$

where again the b, t, s, and a denote bottom, top, side pocket, and atmospheric conditions respectively. The above three equations may be solved iteratively for three unknowns $\bar{P}_b$, $\bar{P}_t$ and $\bar{P}_s$ for given bearing parameters and a given value of E. This determines the values of all flow rates. The result of the pressure field integration

$$W = \iint p dA_v$$

where dA_v is the vertical component of the differential area acted upon at any given point, may be expressed in terms of the nondimensional load

$$\bar{W} = \sqrt{2}\ (\bar{P}_b - \bar{P}_t) \left[1 + \frac{\ell}{L_p}\right]$$

The load capacity is thus determined by

$$W = \bar{W} R L_p P_o.$$

The equations of the preceding analysis are easily programmed and the effects of parameter changes can be studied. In this experiment, bearing stiffness at various supply pressures and oil viscosities was to be studied. Using the above analysis, performance charts were plotted to be compared with the experimental data.

Figures 4 to 6 show the effects of varying oil supply pressure and oil viscosity on the load carrying capabilities of the hydrostatic journal bearing. The parameters used are those of the bearings which were tested:

axial pocket length = 8.255 cm (3.250 in.)
circumferential pocket length = 9.492 cm (3.737 in.)
axial land width = 0.483 cm (0.190 in.)
circumferential land width = 1.016 cm (0.400 in.)
journal radius = 6.35 cm (2.500 in.)
radial clearance = 0.0064 cm (0.0025 in.)
orifice diameter = 0.178 cm (0.070 in.)
orifice discharge coefficient = 0.70

Figure 4 shows the effects of varying the supply pressure to the bearing. The load capacity is greatest at high supply pressures and decreases with decreasing supply pressure. Load capacity changes more rapidly with eccentricity ratio at higher pressures, which means that the bearing stiffness is higher. Bearing stiffness is defined as the change in load capacity divided by the change in radial displacement. This corresponds to the slope of the load capacity vs eccentricity ratio curve.

Figure 5 shows the effects of varying oil viscosity while holding a constant supply pressure. At high eccentricity ratios (greater than 0.8), load capacity is increased by decreasing oil viscosity. In general, the opposite is true at lower eccentricity ratios. For viscosities 2.2 x 10^{-6} reyns and above, bearing stiffness decreases with increasing eccentricity ratio. At lower viscosities, the bearing stiffness increases and then decreases.

Figure 6 depicts the same data as Figure 5 with viscosity as the abscissa. This plot gives a different view of the effects of viscosity on bearing performance. Maximum load capacity is shown to be dependent upon both viscosity and eccentricity ratio. No single viscosity gives maximum load capacity at all eccentricity ratios. It is also evident that as eccentricity ratio increases, the bearing load capacity becomes more sensitive to changes in oil viscosity.

Table 1
Stiffness Ratios, Experimental/Theoretical

Supply Pressure psi	Spring Constant Ratio KExperimental/KTheoretical	KTheoretical (lb/in.)x10^{-6}
600	0.940	2.91
500	0.833	2.46
400	0.674	1.88
300	0.558	1.31

Bearing oil temperature = 145°F

Bearings built to these specifications were installed and successfully operated under all design parameters. As time went on, some degradation in performance was noted so it was decided to test these bearings for stiffness. Such a test involved the installation of hydraulic cylinders to provide load along with instrumentation to accurately measure load and deflection. The results of these tests are shown in Table 1.

The experimental data gives stiffness values lower than those predicted theoretically. The correlation between experimental and theoretical values with regard to changes in supply pressure and viscosities is not as good as expected, although general trends were supported. Several possibilities for the somewhat poor correlation exist.

First, inspection revealed electrical pitting on the bearing lands and journal. The effects from this are enough to significantly affect bearing operation. This pitting tends to increase the effective radial clearance of the bearings and

would decrease load capacity and stiffness. The theoretical analysis assumes that the bearing is symmetrical. The pitting violates this assumption and the actual results could be expected to differ from the predicted.

Bearing Redesign

Having an excellent theoretical and experimental background available, it was decided to investigate the possibility of changing the bearings from the stainless steel backed babbitt to a high pressure laminated (G-9) fiberglass cloth reinforced melamine-formaldehyde resin composite. The new melamine material being a good insulator would solve the electrical pitting problem and reduce the circulating currents and losses through the bearings.

Two questions arose concerning the application of this material for hydrostatic bearings. First, would the melamine absorb oil, and if so, would dimensional stability or strength be affected? Second, would the velocities and shear forces associated with flow across the lands of the hydrostatic bearing cause premature erosion or wear?

Preliminary tests were conducted to answer each of these questions. Time did not permit a thorough investigation using a large number of samples, however, sufficient experimentation was conducted to assure a reasonable chance of success using melamine.

For the oil soak tests, cylindrical samples 0.69 in. in diameter by 0.50 in. long were soaked in oil for a total of 497 hours. No degradation of the samples could be detected.

For the land erosion test, a diametral clearance of 0.0035 in. was selected. The test fixture was sized so that the pressure drop across all flow restrictions was small in comparison to the drop across the lands. Supply pressures of 550-650 psi were used with the nominal being 600. Oil temperatures varied between room temperature and 160°F. The test conditions were representative of those an actual hydrostatic bearing would experience. The land height was approximately the same as that of the current hydrostatic bearings and the land width was about half the width of the lands in the bearings now installed in the 5 MJ generator. One sample was flow tested for over 40 hours and the flow rate checked periodically as an indication of wear. The flow rate was checked by simply measuring the weight of the oil discharged into a container during 2 1/2 minutes. The same conditions of temperature and pressure were used for each flow check, that is T = 120°F, p = 600 psig. Some particles were observed inside the melamine sample during examinations between flow tests. These particles when examined under a microscope were similar to those taken from filter material. They did not look like similar particles taken from the melamine. Flow test results did not indicate that erosion or dimensional changes had taken place.

From these tests and the theoretical model the melamine hydrostatic bearing was obviously the best choice; therefore, it was fabricated and installed in the machine on both radial bearing locations. After installation, these bearings operated as designed for a period of two years during which the machine was operated in the pulsed mode as a part of ongoing research when power was needed.

After a little over two years operation these bearings had changed substantially in performance. Flow tests revealed an increase in clearance to the point that the bearings no longer had sufficient radial stiffness to withstand the forces produced by applying full field strength. What had happened was a progressive step-by-step failure mechanism producing thermal creep and wear from hot spots undergoing thermal runaway.

The bearing shells (one cm thick) were tightly clamped in a rigid stainless steel housing such that the full oil pressure was applied to the shell outside diameter as shown in Figure 7. A solid stainless steel shaft was used as a current conductor thus receiving relatively large diametral changes (~0.1 mm) on each pulse due to the I^2R resistive heating of the shaft. Operation in the pulsed mode is characterized by initial start-up with all materials at the same temperature then as speed is increased the bearing temperature rises gradually over a period of several minutes. Once the rotor is up to the desired speed an electrical pulse is initiated by closing a switch to the load. This initiates a very rapid rise in the shaft temperature over a period of only a few seconds with very little rise in bearing and housing temperature.

This mode of operation combined with the low modulus, high thermal expansion melamine resulted in a temporary loss of clearance which increased shaft heating thereby further reducing the bearing clearance until a rubbing condition existed between the bearing and shaft. Perhaps the best way to describe this condition is a thermal runaway.

Experiences similar to this have been observed in electrical brushes rubbing at high surface speeds. On an electrical brush, as in a bearing making contact, the heating occurs only at selected spots. As these spots heat they expand rapidly relative to the surrounding material thereby making them rub even harder and get hotter. This phenomenon has been referred to as thermal mounding.[1] It is a runaway condition at a local point. Upon cooling, the thermal mound becomes a depression because of wear and creep. Further operation after cooling results in another contact at another location.

Distortion of the bearing shell occurred due to the relatively large outer pressure (up to 1000 psi) combined with the thermal runaway as depicted in Figure 7. Some misalignment of the housings aggravated the degraded oval-shaped and and distorted bearing condition in addition to the thermal problem. At this point it was decided that melamine was not a good choice for this bearing as originally thought and it would be replaced with a more conventional design.

The third generation of hydrostatic bearings (Figure 8) which are currently in the machine, addressed these and other problems. A conventional bronze bearing insert with a hardened steel shaft sleeve was designed. The insert was insulated from a shrunk on steel housing with a layer of flame sprayed aluminum oxide ceramic. The bearing has six pockets and is orifice compensated. By tapering the journal bearing as shown in Figure 9 an adjustable clearance was obtained. Table 2 shows the bearing characteristics.

These bearings are now in the machine and it is operating satisfactorily. An impending rebuild to upgrade the electrical characteristics will probably use these same bearings.

Table 2
Redesigned Hydrostatic Bearing Characteristics

Oil Viscosity cp (Reyn)	Radial Clearance mm (in.)	Load N(lb)	Stiffness N/m (lb/in.)	Flow Liter/min (gpm)	Total Loss kW (hp)
62.1 (9×10^{-6})	0.102 (0.004)	3.47×10^4 (7800)	1.70×10^8 (0.972×10^6)	15.7 (4.16)	20.4 (27.4)
13.8 (2×10^{-6})	0.038 (0.0015)	1.24×10^4 (2781)	8.91×10^8 (5.09×10^6)	8.25 (2.18)	9.10 (12.2)

Conclusion

The use of hydrostatic bearings in an experimental homopolar pulsed power generator has been a good design choice. They have provided all of the desired features such as low shaft friction at zero speed, low losses at high speed, high radial stiffness and low circulating currents. In addition the ability to change their characteristics by external or simple means such as changing oil, changing supply pressure and changing orifice restrictor has made them an excellent choice in a research machine.

When looking back at the selection of melamine for these bearings it now seems quite obvious why it would not be a good choice. This type of design error could have been avoided by the use of conventional materials, but at the time it was selected, hydrostatic bearing theory did not predict this error.

Acknowledgements

The authors wish to acknowledge the experimental and analytical assistance of Drs. K. M. Tolk and R. C. Swanson as well as the support of the U. S. Department of Energy for the development of hydrostatic bearings for the homopolar generator.

References

1 Marshall, R. A., "The Mechanism of Current Transfer in High Current Sliding Contacts," Wear 37 (1976), pp. 233-240.

2 Weldon, W. F., Driga, M. D., Woodson, W. W., Rylander, H. G., "The Design, Fabrication, and Testing of a Five Megajoule Homopolar Motor-Generator," Proceedings: International Conference on Energy Storage, Compression, and Switching, Torino, Italy, November 5-7, 1974.

3 Grant, G. B., Featherston, W. M., Keith, R. E., Weldon, W. F., Rylander, H. G., Woodson, H. H., "Homopolar Pulse Resistance Welding, A New Welding Process - based on the unique electrical characteristics of pulsed homopolar generators," American Welding Society, 60th Annual Meeting, Detroit, Michigan, April 2-6, 1979.

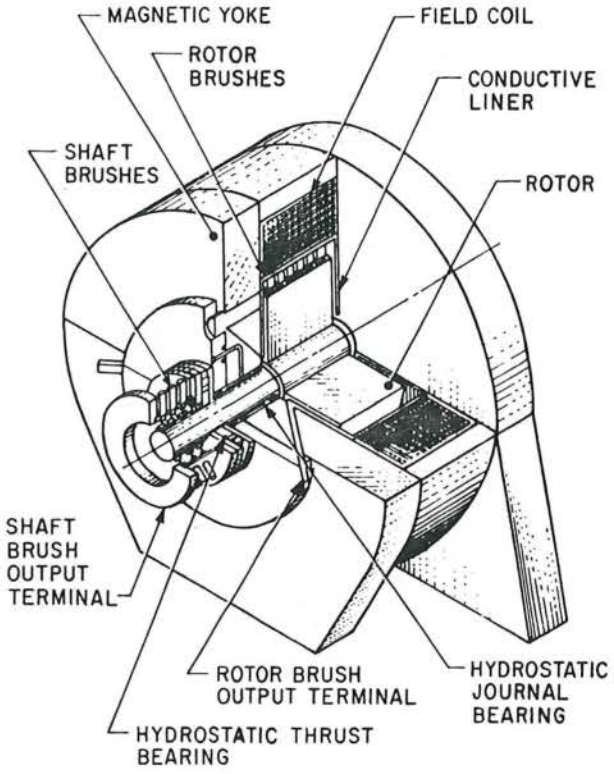

Figure 1: Schematic of 5 MJ Homopolar Machine

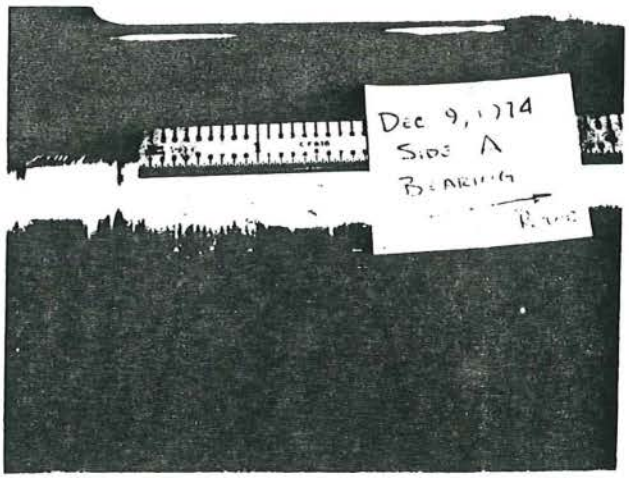

Figure 2: Electrical Pitting on Bearing Lands Side A

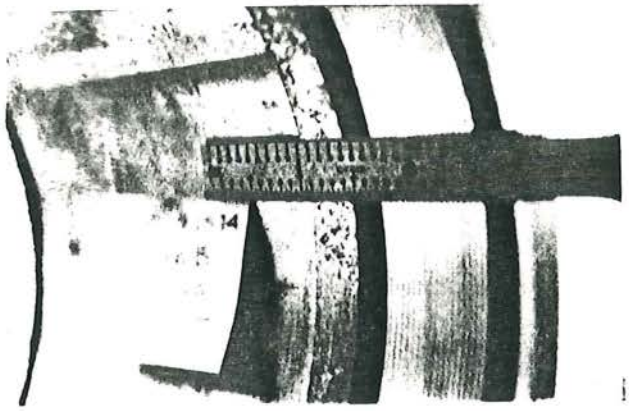

Figure 2: Electrical Pitting on Bearing Lands
Side B

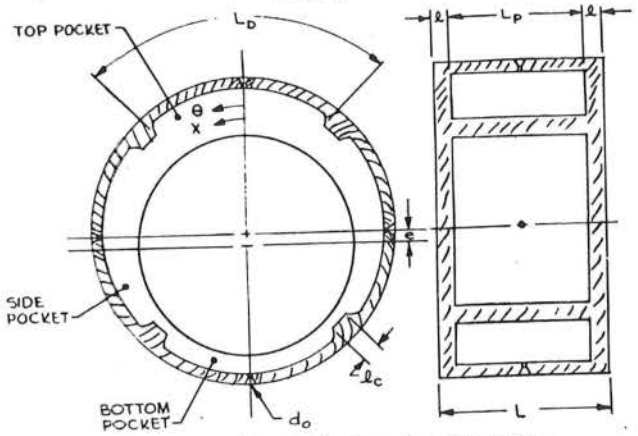

Figure 3: Hydrostatic Bearing Geometry

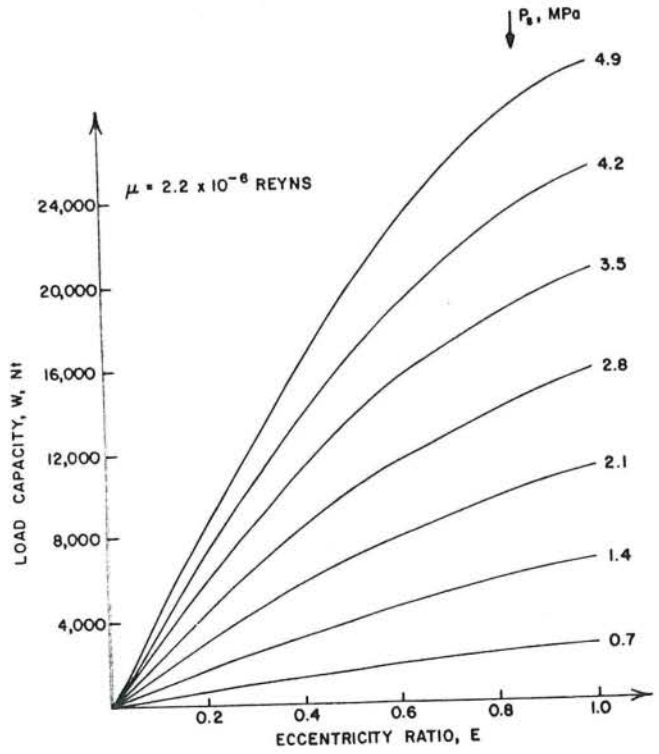

Figure 4: Load Capacity With Varying Supply Pressure

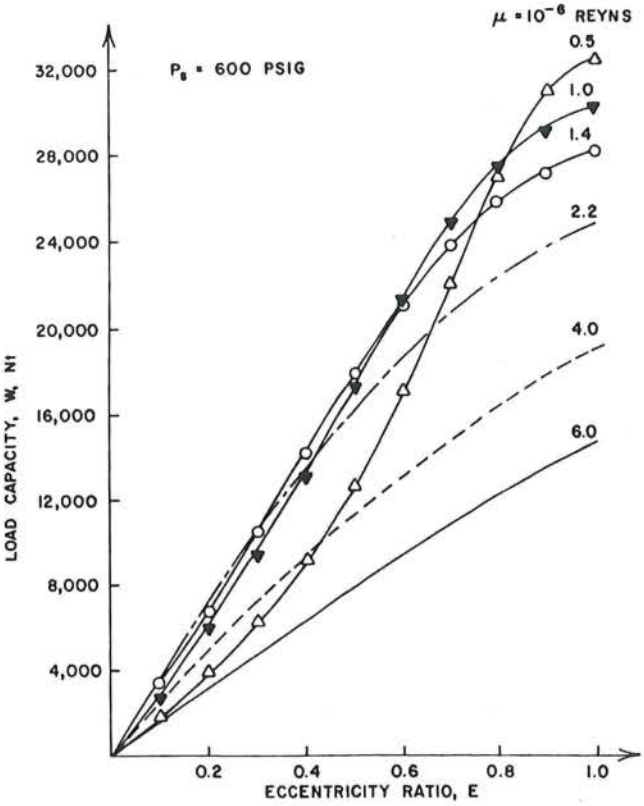

Figure 5: Load Capacity for Various Viscosities

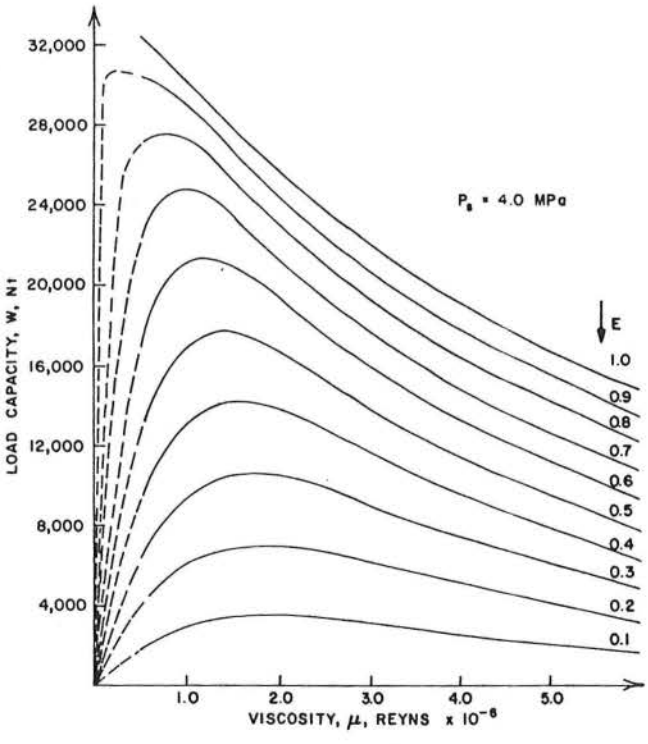

Figure 6: Load Capacity vs E & μ

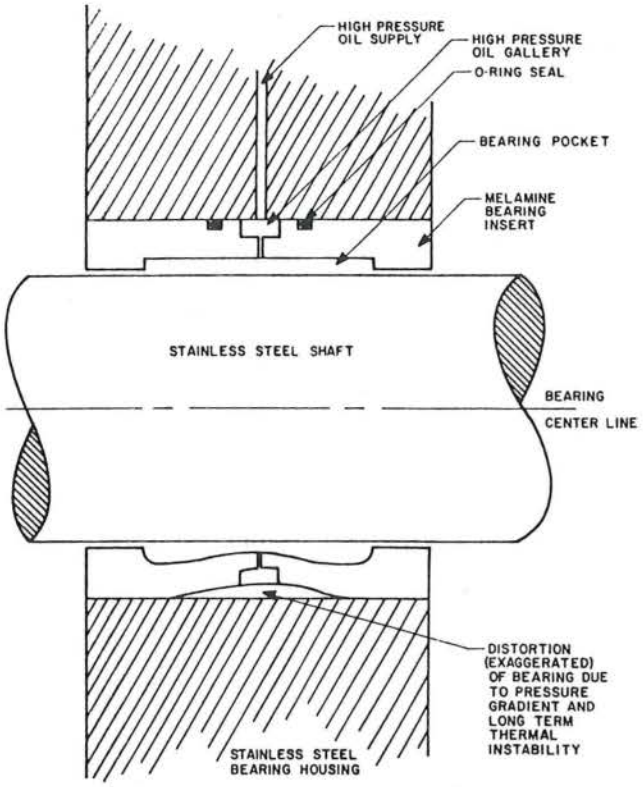

Figure 7: Melamine Bearing With Distortion

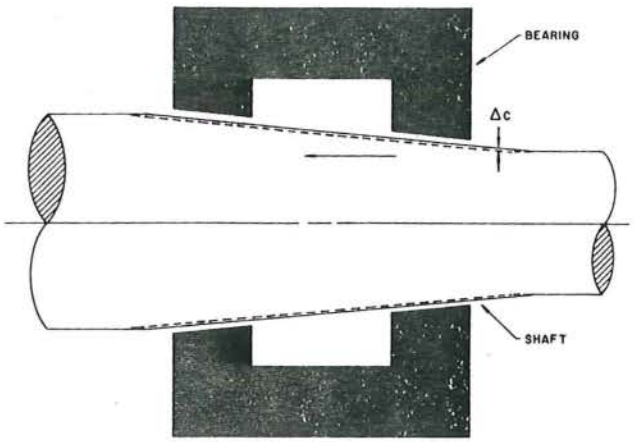

Figure 9: Tapered Shaft and Bearing

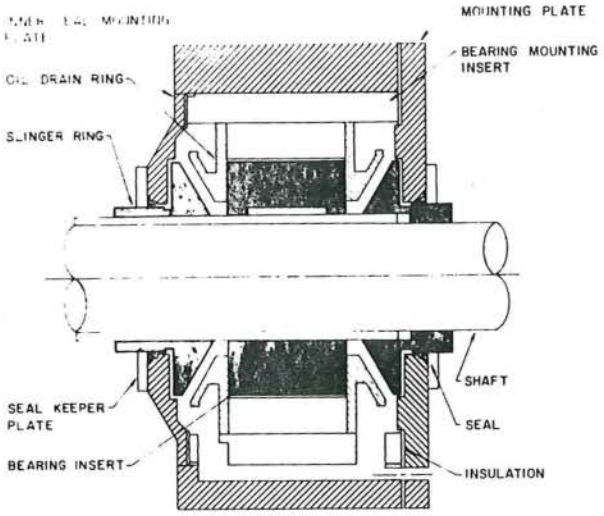

Figure 8: Redesigned Hydrostatic Journal Bearing